CONTRAST MEDIA & MOLECULAR IMAGING

Received: 4 March 2011, Revised: 26 October 2011, Accepted: 30 October 2011, Published online in Wiley Online Library: 2012

(wileyonlinelibrary.com) DOI: 10.1002/cmmi.493

Mn-alginate gels as a novel system for controlled release of Mn^{2+} in manganese-enhanced MRI

Ýrr A. Mørch[a]*, Ioanna Sandvig[b], Øystein Olsen[c], Ivan Donati[d], Marte Thuen[b], Gudmund Skjåk-Bræk[a], Olav Haraldseth[b,e] and Christian Brekken[b]

The aim of the present study was to test alginate gels of different compositions as a system for controlled release of manganese ions (Mn^{2+}) for application in manganese-enhanced MRI (MEMRI), in order to circumvent the challenge of achieving optimal MRI resolution without resorting to high, potentially cytotoxic doses of Mn^{2+}. Elemental analysis and stability studies of Mn-alginate revealed marked differences in ion binding capacity, rendering Mn/Ba-alginate gels with high guluronic acid content most stable. The findings were corroborated by corresponding differences in the release rate of Mn^{2+} from alginate beads *in vitro* using T_1-weighted MRI. Furthermore, intravitreal (*ivit*) injection of Mn-alginate beads yielded significant enhancement of the rat retina and retinal ganglion cell (RGC) axons 24 h post-injection. Subsequent compartmental modelling and simulation of *ivit* Mn^{2+} transport and concentration revealed that application of slow release contrast agents can achieve a significant reduction of *ivit* Mn^{2+} concentration compared with bolus injection. This is followed by a concomitant increase in the availability of *ivit* Mn^{2+} for uptake by RGC, corresponding to significantly increased time constants. Our results provide proof-of-concept for the applicability of Mn-alginate gels as a system for controlled release of Mn^{2+} for optimized MEMRI application.

Keywords: alginate; manganese-enhanced MRI; controlled release; optic nerve; intravitreal injection; ion-binding; retina; retinal ganglion cell axons

1. INTRODUCTION

Alginate, an unbranched polysaccharide composed of guluronic (G) and mannuronic acid (M), is widely used in medicine owing to its unique ability to form a gel at physiological conditions in the presence of divalent cations like Ca^{2+}, Ba^{2+} and Mn^{2+}. In the polymer chain, the monomers are arranged in a block-wise manner as GG-blocks, MG-blocks or MM-blocks of various lengths. Although the importance of G-blocks in the gel-forming process is widely acknowledged, more recent studies (1–3) have shown that the MG-blocks also play an important role in the formation of stable hydrogels. Hence, the gelling properties of alginates are highly dependent on the total composition and arrangement of the monomers in the polymer chains. However, as alginate's affinity to divalent ions differs greatly [in the order $Ba > Ca >> Mn$ for naturally occurring alginates (4,5)], the choice of ions is also of utmost importance (6). It is well known that the binding between guluronic acid residues and Ca or Ba ions is characterized by strong and specific autocooperativity (7). On the other hand, the binding between uronic acid residues in alginate and transition metals like Mn has been characterized by a complex formation in which only the carboxyl groups are coordinated to the metal ions (8).

Ionically crosslinked alginate hydrogels tend to swell and dissolve at physiological conditions mainly caused by the gel network sensitivity towards chelating compounds and/or non-gelling cations such as sodium and magnesium. The divalent crosslinking ions will be released in competition with non-gelling ions, dissolving the junctions in the network. At the same time, given the different valence of crosslinking ions (e.g. Ca^{2+}, Ba^{2+}) and Na^{+}, each divalent ion will be replaced with two Na^{+}, thus increasing the osmotic pressure within the gel network. Both of these effects contribute to swelling and destabilization of the hydrogel network. Swelling can be reduced by using alginate

* *Correspondence to: Ýrr A. Mørch, Department of Biotechnology, NTNU, Sem Sælands vei 6/8, NO-7491 Trondheim, Norway.*
E-mail: yrr.morch@ntnu.no

a *Ý. A. Mørch, G. Skjåk-Bræk*
Department of Biotechnology, Norwegian University of Science and Technology, Trondheim, Norway

b *I. Sandvig, M. Thuen, O. Haraldseth, C. Brekken*
MI Lab and Department of Circulation and Medical Imaging, Norwegian University of Science and Technology, Trondheim, Norway

c *Ø. Olsen*
Department of Technology, Sør-Trøndelag University College, Trondheim, Norway

d *I. Donati*
Department of Biochemistry, Biophysics and Macromolecular Chemistry, University of Trieste, Trieste, Italy

e *O. Haraldseth*
Department of Radiology, St Olav's Hospital, Trondheim, Norway

with a high content of long guluronic acid blocks (9,10), or by using divalent ions with high binding affinity to alginate (such as Ba^{2+}) (10–12). As manganese has low affinity to alginate and consequently does not form stable hydrogels, a limited amount of research has been dedicated to Mn-alginate gels. Conversely, we hypothesize that this lack of stability may be used for the purpose of a slow release system of Mn^{2+} for magnetic resonance imaging.

Manganese-enhanced magnetic resonance imaging (MEMRI) is an imaging modality that utilizes the unique properties of manganese ions (Mn^{2+}) as an intracellular and functional contrast agent in T_1-weighted imaging. In the central nervous system (CNS), Mn^{2+} enter neurons through L-type voltage-gated Ca^{2+} channels (13), after either systemic delivery or direct injection into the area of interest. Furthermore, Mn^{2+} are paramagnetic and shorten the T_1 spin–lattice relaxation time of surrounding water protons in areas of Mn^{2+} accumulation, yielding high-contrast T_1-weighted MR images (14–16). Given these properties and the fact that various brain tissues, such as the different cortical laminae, display different Mn^{2+} affinity, Mn^{2+} can be utilized as a contrast agent in studies of neuronal architecture (17). Furthermore, increased brain activity results in elevated intracellular uptake of Mn^{2+} via Ca^{2+} channels. As a result, MEMRI can also be utilized in studies of functional brain activity (18,19). In addition to the above, MEMRI can be used for *in vivo* tracing of CNS axon tracts (15,17,20–22). Upon entry into neurons, Mn^{2+} are sequestered in the endoplasmic reticulum, and subsequently transported along axonal microtubules to the synaptic cleft, where they are released and trans-synaptically relayed to other neurons (15,20,23). The specific properties of Mn^{2+} render MEMRI particularly relevant in experimental models of CNS damage and repair, as it enables longitudinal monitoring of damaged and regenerating neuronal pathways (21,22,24,25) and connectivity *in vivo* (26–28).

Nevertheless, a major consideration in applying MEMRI is the potential risk of Mn^{2+}-induced cytotoxicity (29) associated with high and/or repeated doses of Mn^{2+}. Previous studies demonstrated that increased Mn^{2+}-induced signal enhancement, which is desirable in terms of optimal image resolution, can be obtained with higher doses of Mn^{2+} (30), followed by the caveat that neuronal viability may be significantly compromised (21,31,32). It has been demonstrated, though, that there is a plateau of maximum Mn^{2+} entry into neurons, which indicates that increased Mn^{2+}-induced signal enhancement is contingent on the duration of Mn^{2+} availability, rather than on Mn^{2+} dose (30). It follows that regulation and adjustment of Mn^{2+} release to the neuronal uptake threshold should dramatically reduce exposure of neurons to Mn^{2+}, a manipulation that should be possible with the use of tailor-made alginate matrices saturated with Mn^{2+} for targeted, controlled release of Mn^{2+}.

The purpose of this study was to analyse the binding and release of manganese ions from different types of alginate gels. We aimed to design a system for slow and controlled release of Mn^{2+} as a contrast agent in MRI. The release of manganese from alginate gels using two commercial alginates (a high-M and high-G alginate) as well as alginates of extreme composition (polyM, polyMG and polyG alginate) and different combinations of divalent ions was studied. Mn^{2+} release from single alginate beads *in vitro* was imaged in real time using T_1-weighted MRI at 7 T and relevant time constants were obtained. Furthermore, *ivit* injection of Mn-alginate beads in rat was performed to obtain MEMRI of the rat retina, optic nerve and contralateral superior colliculus at 2.35 T, thus providing proof-of-concept regarding the utility of Mn-alginate gels for controlled release of Mn^{2+} for MEMRI.

2. MATERIALS AND METHODS

2.1. Alginates

Five different alginate samples were used in the present study. Two commercially available alginates and three alginates of extreme composition representing the different blocks in alginate were obtained from FMC biopolymer and Sigma Chemicals, respectively: (i) high-G alginate from *Laminaria hyperborea* (67% G, intrinsic viscosity 620 ml g^{-1}) and (ii) high-M alginate from *Macrocystis pyrifera* (40% G, intrinsic viscosity 820 ml g^{-1}). (iii) A polymannuronan alginate (polyM, 0% G, intrinsic viscosity 800 ml g^{-1}) was produced by an epimerase-negative mutant ($AlgG^-$) of *Pseudomonas fluorescens* (33). (iv) A strictly alternating (polyMG) alginate (46% G, 0% GG, intrinsic viscosity 700 ml g^{-1}) and (v) a polyguluronan alginate (polyG, 88% G, intrinsic viscosity 1150 ml g^{-1}) were achieved by epimerizing the bacterial polyM alginate with the C-5 epimerases AlgE4 and AlgE6, respectively, as reported elsewhere (34). For circular dichroism (CD) measurements, the polyG sample used was an acid-insoluble fraction of alginate (35) enriched in G blocks (94% G) with a degree of polymerization (DPn) of 18.5.

2.2. Alginate gel beads

Alginate gel beads were formed by dripping a 1.8% (w/v) solution of Na-alginate (filtered through 0.8 μm filters, dissolved in ion free water) into solutions containing divalent cations (gelling solutions). The solutions contained 0.1 M $MnCl_2$ + 1 mM $BaCl_2$ or 0.1 M $MnCl_2$ + 10 mM $CaCl_2$. A syringe pump was utilized in order to form evenly sized, spherical beads.

2.3. Alginate gel cylinders

Alginate samples (1.8% w/v) were placed into hollow plastic cylinders (inner diameter, 16 mm; height, 18 mm) with a dialysis membrane (MWCO 12 000–14 000) attached at both ends. The cylinders were kept in gelling solution (0.1 M $MnCl_2$ + 1 mM $BaCl_2$ or 0.1 M $MnCl_2$ + 10 mM $CaCl_2$) for 48 h.

2.4. Elemental analysis

Alginate beads were gelled in solutions containing the various amounts of divalent ions for 24 h, and washed three times in saline (<1 min) to remove excess ions. The beads were dried gently on a paper cloth and placed in polylpropylene tubes (60 ml, Sarstedt) before tri-Na-citrate (50 mM, Merck) was added to dissolve the gels. Elemental analysis was performed by inductively coupled plasma mass spectrometry (High-resolution ICP-MS, Element 2, Thermo Scientific) to measure the content of Mn, Ba and Ca in the gel after dissolution in Na citrate. The stability of the different gels towards ion-exchange (and hence Mn^{2+} release) was studied by monitoring the dimensional swelling of the gel beads upon incubations in saline (0.9% NaCl). The saline solution was changed every hour.

2.5. Circular dichroism spectroscopy

Circular dichroic spectra of the sodium form of polyM, polyG and polyMG ($c \approx 3 \times 10^{-3}$ monomol l^{-1}) were recorded in deionized

water with an Olis DSM 1000 spectropolarimeter. A quartz cell of 1 cm optical path length was used. The integration time was a function of high voltage, and bandwidth was 1 nm. Four spectra corrected for the background were averaged for each sample. The spectrum of each sample was recorded prior to and after the addition of $Mn(ClO_4)_2$, with an increasing $[Mn^{2+}]/[Polym_{ru}]$ (Rj) ratio.

2.6. Viscosity measurements

Specific capillary viscosity was measured at 25 °C by means of a Schott-Geräte AVS/G automatic apparatus and an Ubbelohde type viscometer upon addition of $Mg(ClO_4)_2$, $Mn(ClO_4)_2$ and $Ca(ClO_4)_2$ at different values of the R_j ratio ($R_j = [M^{2+}]/Cp$). A 3×10^{-3} monomol l^{-1} polymer solution (Cp) in 0.05 M $NaClO_4$ was used in all cases. All solutions were filtered through Millipore filters (0.45 μm) prior to use.

2.7. *In vitro* MRI of Mn^{2+} release from single alginate beads

MRI was performed at 7 T on a Bruker Biospec 70/20 AS with BGA-12 400 mT m^{-1} gradients. A 72 mm volume resonator was used for RF transmit and receive. Single alginate beads (diameter approximately 4 mm) stored in gelling solution were rapidly (<1 min) washed three times in 3 ml 0.9% NaCl and suspended by a nylon tulle sling inside empty 5 ml glass vials connected to a custom-made fluid-transfer line. The glass vials with the alginate beads were subsequently placed inside the scanner. The MRI protocol consisted of tri-axial 2D scout scans, and an evolutionary 2D T_1-weighted sequence up to 24 h after alginate bead immersion into 5 ml 0.9% NaCl solution inside the magnet via the above-mentioned fluid-transfer line. The specific protocol was repeated three times for each type of alginate bead. Key parameters for MRI included:

- 2D MSME (T_1) scout scan: echo time, 11 ms; repetition time, 200 ms; field of view, 50 × 50 mm; matrix, 128 × 128; slice thickness, 1 mm (three orthogonal slices); number of excitations, 1; acquisition time, 25 s.
- 2D MSME (T_1) evolution scanning: echo time, 8.1 ms; repetition time, 500 ms; field of view, 30 × 40 mm; matrix, 128 × 64; slice thickness, 1 mm; number of excitations, 1; six frames per hour during 24 h.

2.8. *In vivo* MRI of Mn^{2+} release from alginate beads

All experimental procedures involving animals were approved by the appropriate ethics committee and were in accordance with national, regional and site guidelines that apply. During surgery and *in vivo* MRI, rats were anesthetized with a 1:1:2 mixture of Hypnorm–Durmicum–sterile water subcutaneously (2.5 ml kg^{-1}). Small high-G Mn-alginate beads (diameter approximately 500 μm) were formed by dripping a 1.8% (w/v) alginate solution into a 1 M $MnCl_2$ + 1 mM $BaCl_2$ gelling solution using an electrostatic bead generator. Approximately 20 beads were unilaterally implanted into the vitreous body of adult Fischer rats ($n = 4$) through the ora serrata using a 25 G needle. MRI was performed 24 h after alginate bead implantation using a 2.35 T Bruker Biospec Avance DBX-100 (Bruker Biospin) with a 72 mm volume coil for transmission and an actively decoupled rat head surface coil for receive-only. Anesthetized rats lay prone in a dedicated animal bed heated with warm air at 37 °C. After acquiring a scout scan, a 3D data set of the entire rat head was obtained using a T_1-weighted 3D low-flip-angle shot (FLASH) gradient echo sequence with echo time, 4.2 ms; repetition time, 15 ms; flip angle, 25°; field of view, 50 × 50 × 20 mm^3; matrix, 256 × 256 × 64 (resolution, 195 × 105 × 312 μm^3) with eight averages and a total scan time of 33 min

2.9. Model of Mn^{2+} release and analysis of MRI data

A compartment model of the system (Fig. 1A) was used to describe the release of Mn^{2+} from the dissolving alginate beads and the subsequent increase in Mn^{2+} concentration in the surrounding physiological saline solution. Under the assumption of mass conservation, the rate of change of the amount of bound Mn^{2+} in the alginate gel beads was described by:

$$\frac{dQ_1}{dt} = -k_1 Q_1, \quad Q_1(0) = Q_{01} \tag{1}$$

where Q_1 is the time dependent amount of bound Mn^{2+}, k_1 the release rate coefficient and Q_{01} the initial amount of bound Mn^{2+} in the alginate gel beads. The rate of change of the amount of unbound Mn^{2+} was described by:

$$\frac{dQ_2}{dt} = -k_2 Q_2, \quad Q_2(0) = Q_{02} \tag{2}$$

where Q_2 is the time-dependent amount of unbound Mn^{2+}, k_2 the release rate coefficient and Q_{02} the initial amount of unbound Mn^{2+} in the alginate gel beads. The rate of change of the amount of Mn^{2+} in the saline solution, Q_3, surrounding the alginate gels during the MR experiment, was described by:

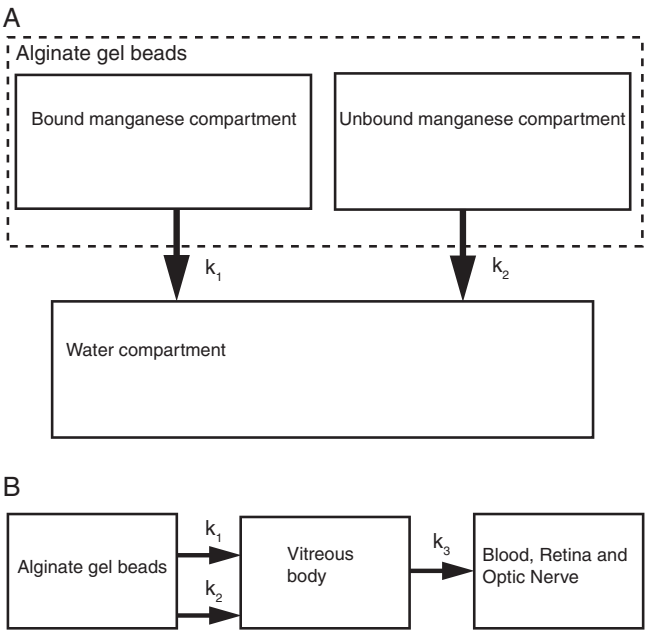

Figure 1. (A) The release of Mn^{2+} from alginate gel beads to the surrounding water during the MR experiment was described by a compartment model. We assumed both bound and unbound Mn^{2+} present in the alginate gel beads which were released with release rates k_1 and k_2, respectively. (B) Compartment model for simulation of intravitreal Mn^{2+} concentration. We assumed Mn^{2+} to be released with two release rate (k_1 and k_2) from the alginate gel bead and into the vitreous body compartment, where it was cleared with the rate k_3. In a biological system the route of Mn^{2+} clearance from the vitreous body probably is by vascular transudation and anterograde transport within RGC axons.

$$\frac{dQ_3}{dt} = k_1 Q_1 + k_2 Q_2, \quad Q_3(0) = 0 \tag{3}$$

Solving this set of simultaneous first-order linear differential equations [eqns (1)–(3)] yielded

$$Q_3(t) = Q_{01}[1 - \exp(-k_1 t)] + Q_{02}[1 - \exp(-k_2 t)] \tag{4}$$

If we assume all Mn^{2+} to be transferred to the water compartment, eqn (4) can be written:

$$C(t) = C_{01}[1 - \exp(-k_1 t)] + C_{02}[1 - \exp(-k_2 t)] \tag{5}$$

where *C(t)* is the time-dependent Mn^{2+} concentration in the saline solution compartment, C_{01} the contribution to the total concentration of Mn^{2+} from the bound Mn^{2+} compartment and C_{02} the contribution to the total concentration of Mn^{2+} in the saline solution compartment from the unbound Mn^{2+} compartment. Furthermore, the time constant for release was defined as $\tau_i = 1/k_i$ and a linear relationship between Mn^{2+} concentration and MR signal intensity (SI) approximated. In addition, the baseline signal from water was added to obtain a model of the time-dependent MEMRI signal:

$$S(t) = S_0 + S_1[1 - \exp(-t/\tau_1)] + S_2[1 - \exp(-t/\tau_2)] \tag{6}$$

where S_0 is the baseline saline solution signal, S_1 and S_2 the portion of the signal caused by the total release of bound and unbound Mn^{2+}, and τ_1 and τ_2 the time constants for release of Mn^{2+} from the bound and unbound Mn^{2+} compartments, respectively.

The MEMRI datasets were corrected for differences in receiver gain and reconstruction scaling. Dynamic SI curves were calculated from a ROI placed close to the rim of the container but excluding the alginate beads in each frame. The time constants for Mn^{2+} release were extracted by fitting the SI model [eqn (6)] to mean SI curves. To invalidate a bi-exponential model, a mono-exponential function was fitted to the data and compared with the bi-exponential fit. Curve extraction and data fitting was performed using in-house developed software and the Curve Fitting Toolbox™ (Matlab version 7.8.0, Mathworks Inc., Natick MA, USA). Confidence bounds of the estimated time constants were calculated within the Curve Fitting Toolbox™, which utilizes the inverse R factor from QR decomposition of the Jacobian, the degrees of freedom for error, and the root mean squared error.

2.10. Simulation of *ivit* Mn^{2+} concentration

A compartment model (Fig. 1B) was used to simulate the amount of Mn^{2+} in the vitreous body after *ivit* injection of a slow release contrast agent containing both bound and unbound Mn^{2+}. We used the following equation to describe the rate of change of the amount of bound Mn^{2+} in the contrast agent:

$$\frac{dQ_1}{dt} = -k_1 Q_1, \quad Q_1(0) = Q_{01} \tag{7}$$

The rate of change of unbound Mn^{2+} in the contrast agent was described by:

$$\frac{dQ_2}{dt} = -k_2 Q_2, \quad Q_2(0) = Q_{02} \tag{8}$$

The rate of change of the amount of Mn^{2+} in the vitreous body, Q_v, was described by:

$$\frac{dQ_v}{dt} = k_1 Q_1 + k_2 Q_2 - k_3 Q_v, \quad Q_v(0) = 0 \tag{9}$$

where k_3 is the rate coefficient of Mn^{2+} vitreal clearance. This set of simultaneous first-order linear differential equations [eqns (7)–(9)] was solved to calculate the maximum *ivit* Mn^{2+} concentration.

The time constants $\tau_1 = 100$ min and $\tau_1 = 600$ min were used to characterize two slow-release contrast agents with different release rates. In both cases, release of unbound Mn^{2+} was described by the time constant $\tau_2 = 25$ min. The resulting time-dependent *ivit* Mn^{2+} concentration was compared with a bolus injection. The time-dependent *ivit* Mn^{2+} concentration after a bolus injection was described by a mono-exponential decay function:

$$C_v(t) = C_{01} \exp(-t/\tau_3) \tag{10}$$

A time constant for vitreal clearance, $\tau_3 = 147$ min, was adapted from Olsen *et al.* (30). The maximum *ivit* Mn^{2+} concentration was calculated for cases where 20, 80 and 100% of the initial amount of Mn^{2+} in the contrast agent was contained in the bound Mn^{2+} compartment.

3. RESULTS

3.1. Binding of divalent ions to alginate

Two naturally occurring alginates and three alginate samples of pure block composition were used to study both the binding of divalent ions in alginate gels and the stability of these hydrogels towards ion exchange, and hence Mn^{2+} release. In order to stabilize Mn-alginate gels, combinations of Mn^{2+}/Ba^{2+} and Mn^{2+}/Ca^{2+} were used. As the stability of Mn-alginate gels towards ion exchange *in vivo* will control the release rate of Mn^{2+}, the dimensional swelling of gel beads in physiological saline was studied. The various gels investigated showed great differences with regard to stability (Table 1). Not surprisingly, an alginate with high content of G (high-G, 67%) and with added Ba^{2+} in the gelling solution was found to be least susceptible to ion exchange. However, increasing the G content to almost solely containing G-blocks (polyG, 88%) did not improve the stability, but rather led to enhanced swelling. Gels of high-M and polyMG alginate all dissolved immediately in saline, indicating that, for these gels, most of the Mn^{2+} is released quickly in exchange for Na^+. An alginate of pure mannuronic acid (polyM) did not form gels with either Mn^{2+}/Ca^{2+}, or Mn^{2+}/Ba^{2+}.

If Mn-alginate is to be used for MEMRI purposes, not only the release rate of Mn^{2+}, but also the total amount of Mn^{2+} conserved in the gel upon *in vivo* implantation, are of importance. Following the gelling of alginate, beads were quickly washed in saline and the gels analysed with regard to divalent ion content. The initial amount of Mn^{2+} in alginate gels was found to be quite constant regardless of the type of alginate and secondary ions used. The only exception to this is the combination of Mn^{2+} and Ca^{2+} in polyalternating alginate (polyMG) which in total contains a considerably lower amount of Mn^{2+} (see Table 2). The highest amount of divalent ions

Table 1. Stability of alginate gel beads in 0.9% NaCl upon exchange of saline solution. Values are measured diameter of beads in millimetres. Alginates were of various compositions all with a polymer concentration of 1.8% (w/v). The concentration of ions in the gelling solution was 0.1 M Mn^{2+} and 10 mM Ca^{2+} (Mn/Ca) or 0.1 M Mn^{2+} and 1 mM Ba^{2+} (Mn/Ba). The gels were washed twice in physiological saline solution (3 ml 0.9% for each) to remove excess gelling solution before the diameter was measured in a light microscope. The capsules were transferred to 3 ml of fresh saline solution and kept on stirring for 1 h before the diameter was again measured. The procedure was repeated for beads that were still intact. Beads could not be formed from the polyM alginate

Alginate	Gelling ions	Start	First shift	Second shift	Third shift	Fourth shift	Fifth shift	Sixth shift	Seventh shift	Eighth shift
HighM	Mn/Ca	3.8	Dissolved							
	Mn/Ba	3.8	Dissolved							
HighG	Mn/Ca	4.0	4.3	4.3	4.5	Dissolved				
	Mn/Ba	4.0	4.0	4.0	4.5	4.5	4.6	4.9	4.9	4.9
PolyMG	Mn/Ca	3.0	Dissolved							
	Mn/Ba	3.5	Dissolved							
PolyG	Mn/Ca	4.0	Dissolved							
	Mn/Ba	4.0	4.0	4.0	4.0	Dissolved				

Table 2. Amount of manganese, calcium and barium bound in alginate gels of various compositions measured by ICP-MS. Alginate concentration was 1.8% (w/v) and concentration of ions in gelling solution was 0.1 M Mn^{2+} + 10 mM Ca^{2+} (Mn/Ca) or 0.1 M Mn^{2+} + 1 mM Ba^{2+} (Mn/Ba). The gels were washed three times in physiological saline solution to remove excess gelling solution and slightly dried on a paper cloth before they were dissolved in Na-citrate. The values are means ± SD of three parallels and corrected for concentration of ions in the solvent

		Moles divalent ion/mole uronic acid			Bound divalent ion (in μg ml^{-1} alginate)			Molar ratio of divalent ions in gel beads
Alginate	Gelling ion	Mn^{2+}	Ca^{+2}	Ba^{2+}	Mn^{2+}	Ca^{+2}	Ba^{2+}	
HighM	Mn/Ca	0.75 ± 0.01	0.187 ± 0.002	0	3713 ± 37	675 ± 6	0	Mn:Ca, 4:1
	Mn/Ba	0.76 ± 0.02	0	0.064 ± 0.001	3743 ± 116	0	794 ± 7	Mn:Ba, 12:1
HighG	Mn/Ca	0.80 ± 0.01	0.22 ± 0.01	0	3953 ± 47	789 ± 20	0	Mn:Ca, 4:1
	Mn/Ba	0.87 ± 0.06	0	0.135 ± 0.004	4319 ± 311	0	1671 ± 47	Mn:Ba, 6:1
PolyMG	Mn/Ca	0.62 ± 0.03	0.147 ± 0.004	0	3076 ± 126	532 ± 14	0	Mn:Ca, 4:1
	Mn/Ba	0.93 ± 0.02	0	0.0148 ± 2 × 10^{-4}	4587 ± 99	0	183 ± 3	Mn:Ba, 63:1
PolyG	Mn/Ca	0.79 ± 0.07	0.24 ± 0.01	0	3916 ± 329	864 ± 27	0	Mn:Ca, 3:1
	Mn/Ba	0.89 ± 0.09	0	0.176 ± 0.003	4391 ± 443	0	2173 ± 42	Mn:Ba, 5:1
PolyM	Mn/Ca				Beads could not be formed			
	Mn/Ba				Beads could not be formed			

(Mn^{2+} and Ca^{2+}/Ba^{2+}) conserved in the gel after a pre-washing step was found in alginates containing long G blocks (polyG and high-G alginate).

To further investigate the binding of Mn^{2+} to the different block structures in alginate at a qualitative level, CD was performed on blocks of G-, MG- and M residues (Fig. 2). Changes in the molar ellipticity upon addition of Mn^{2+} are observed in the CD spectra for G-blocks and MG-blocks, representing the formation of junctions (a higher degree of ordering of the chain) and hence a specific interaction of Mn^{2+} with the polymer. The CD spectra of polyM are in contrast unaffected by the additions of Mn^{2+}, thus indicating a lack of interaction between Mn^{2+} and M-blocks in alginate.

If the binding of divalent ions to alginate results in complex formation, the addition of these ions to dilute alginate solutions will lead to an increase in viscosity. The effect of the additions of Mn^{2+} on the specific viscosity of polyM, polyMG and high-G alginate is given in Fig. 3 and compared with the additions of the non-gelling magnesium ion (Mg^{2+}). Although the differences are small, the gap between Mg^{2+} and Mn^{2+} seems to increase in the order polyM < polyMG < high-G.

Figure 4 illustrates that there are great macroscopic differences between Mn-alginate gels of different block structures. Gels of polyMG alginate were transparent and rigid, while all other alginate samples tested were turbid, soft gels. Gels containing high amounts of G residues (polyG and high-G) were milky white, whereas a high-M alginate was turbid.

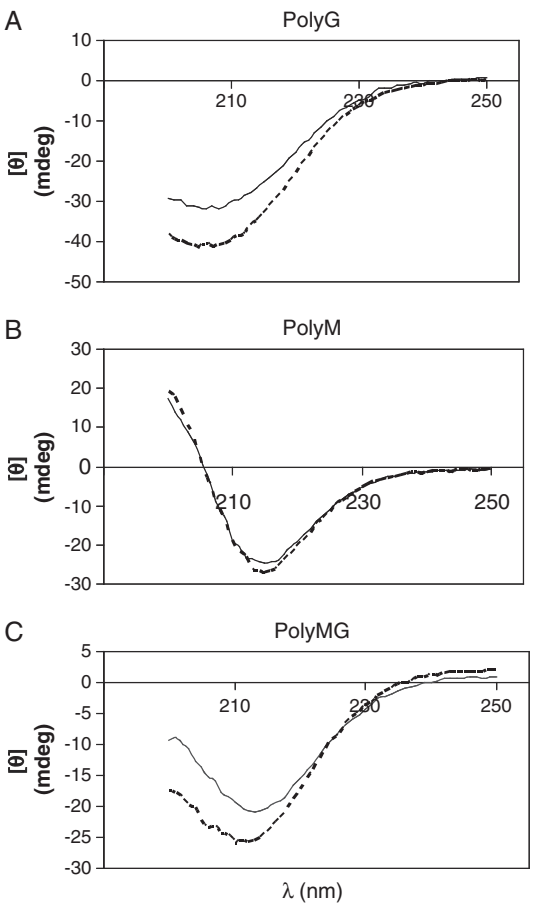

Figure 2. Circular dichroism spectra of (A) polyG, (B) polyM and (C) polyMG given as molar ellipticity as a function of wavelength before (dotted line) and after (continuous line) addition of Mn^{2+} (Mn/polymer repeating unit = 0.5).

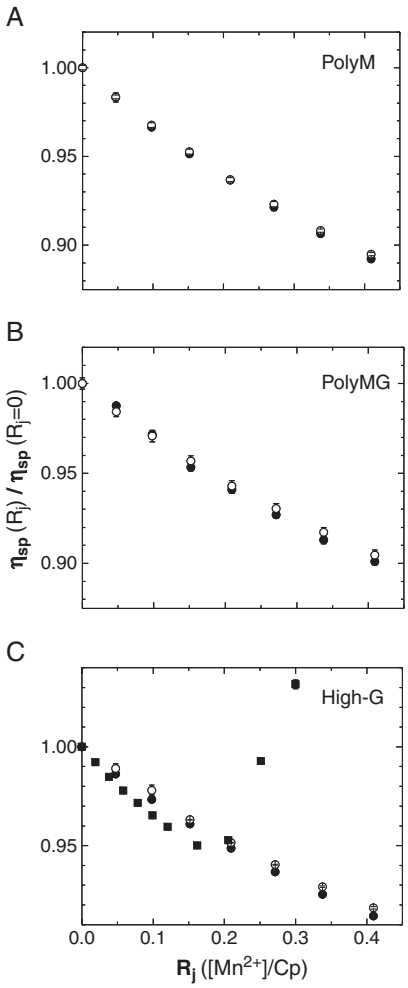

Figure 3. Relative variation of the specific viscosity upon addition of divalent ions [$\eta_{sp}(R_j)$] with respect to the specific viscosity [$\eta_{sp}(R_j = 0)$] of (A) polyM, (B) polyMG and (C) high-G. Legend: (●) Mn^{2+}, (○) Mg^{2+} and (■) Ca^{2+}.

3.2. *In vitro* MEMRI using Mn-alginate

In vitro MEMRI of all the different types of Mn-alginate beads revealed diverse profiles of release of Mn^{2+} from the beads over time (Figs 5 and 6). The dynamic changes of Mn^{2+} concentration in the surrounding water were contingent on Mn-alginate bead type. This is illustrated in Fig. 5, which provides representative examples of controlled release of Mn^{2+} from polyMG Ba/Mn and high-G Ba/Mn alginate beads in saline at three different time points after washing. When Mn^{2+} was released from the alginate beads, the Mn^{2+} concentration in the surrounding water increased, shown as an increase in SI. However, high concentrations of Mn^{2+} can cause signal loss because of the T_2 effect and this was seen in the MEMRI of alginate gel beads at early time points. High-G Ba/Mn alginate retained a high concentration of Mn^{2+} for a longer period of time than the polyMG Ba/Mn sample, seen as prolonged hypointensity of the alginate gel beads (Fig. 5).

Figure 6 shows the best fit of the model [eqn (6)] to the dynamic MEMRI curves of the six different alginate beads. The bi-exponential model of Mn^{2+} release fitted the data well, but

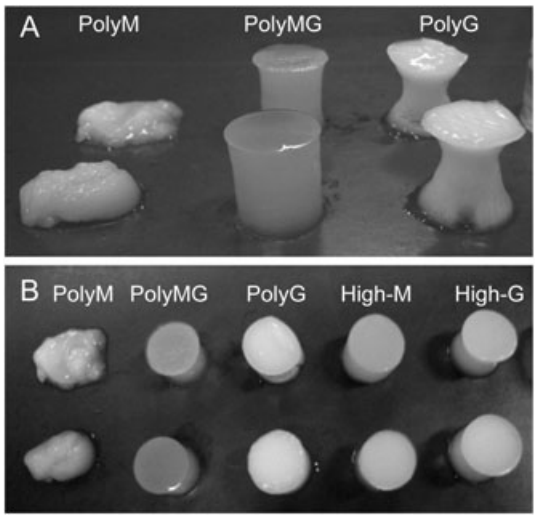

Figure 4. Appearance of Mn-alginate gel cylinders. (A) Alginate samples representing the three block structures in alginate. From left: PolyM, polyMG and polyG. Back: Mn/Ca alginate. Front: Mn/Ba alginate. (B) Alginate cylinders of the various alginate samples (seen from above) used in the present study. From left: polyM, polyMG, polyG, high-M and high-G. Top: Mn/Ca alginate. Bottom: Mn/Ba alginate. Mn-polyMG gels were transparent, strong gels, whereas Mn-polyG gels were milky white, very soft gels. PolyM alginate did not form stable hydrogels with manganese.

polyMG alginate with Ba^{2+} (Fig. 6D) seemed to release large amounts of Mn^{2+} fast, which resulted in a temporary local high concentration in the image plane early in the experiment. These data points were hence removed in the further model fitting. A mono-exponential function was inadequate to describe the fast increase in SI, as the best fit gave large residuals for the early time points for all data sets (data not shown).

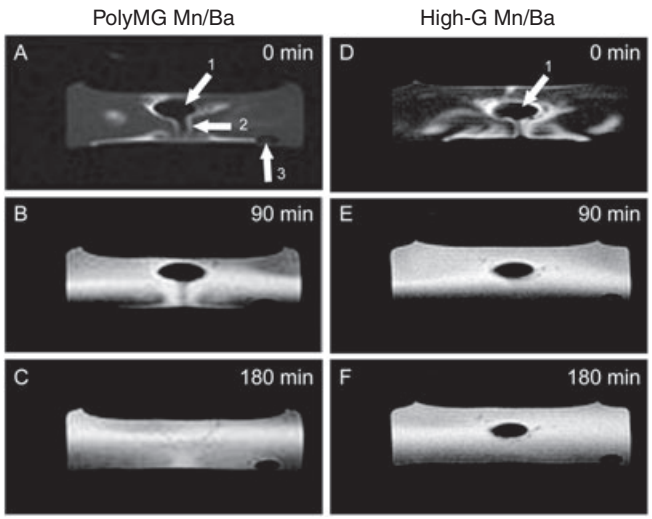

Figure 5. MRI of polyMG Mn/Ba-alginate (A–C) and high-G Mn/Ba-alginate (D–F) beads. The high concentration of Mn^{2+} in the alginate gel beads (1) caused signal loss (T_2 effect) and rapidly released Mn^{2+} flowed downward from the alginate beads early in the experiment (2). After being distributed in the water, the Mn^{2+} concentration sank and caused hyper-intensity in the T_1-weighted images. Note how the Mn^{2+} concentration remained high in high-G Mn/Ba-alginate (D–F), whereas polyMG Mn/Ba-alginate seemed to release Mn^{2+} faster (A–C). The fluid-transfer line used for filling the glass vials is seen in the lower-right corner (3). The bead diameter was approximately 4 mm.

Time constants extracted from the model fit (Fig. 6) are found in Table 3. The model fitting showed that Mn^{2+} was released with two distinct release rates: (i) a slow release rate, corresponding to a long time constant, τ_1 and (ii), a fast release rate, corresponding to a short time constant, τ_2. The short time constant (τ_2) varied marginally between the different groups. By contrast, τ_1 values show great variation (100–700 min) between the groups in the order high-G ≥ high-M > polyMG, increasing upon using Ba^{2+} instead of Ca^{2+} as secondary ion.

The simulation of *ivit* Mn^{2+}concentration (Fig. 7E) showed that using slow release systems with time constants of 100 and 600 min effectively reduces the maximum *ivit* Mn^{2+} concentration. The time constant of 600 min reduced the maximum *ivit* Mn^{2+} concentration to 57, 21 and 15% as the initial amount of bound Mn^{2+} in the contrast agent was set to 20, 80 and 100%, respectively. For the same initial amounts of bound Mn^{2+}, the time constant of 100 min reduced the maximum *ivit* Mn^{2+} concentration to 63, 46 and 44%, respectively. These are significant reductions, considering that maximum *ivit* Mn^{2+} concentration derived from a bolus injection is 100% *in vivo*.

3.3. *In vivo* MEMRI using Mn-alginate

Proof of principle of optic nerve Mn^{2+} enhancement after Mn-alginate bead injection was demonstrated by intravitreal (*ivit)* injection of high-G Mn/Ba-alginate beads in rats. Figure 7(A–D) shows significant enhancement of the retina, optic nerve and contralateral superior colliculus 24 h post-*ivit* injection.

4. DISCUSSION

4.1. Binding and release of Mn^{2+}

If a controlled release system for Mn^{2+}-enhanced MRI is to be designed, knowledge on the ion binding capacity to the different block structures in alginate is fundamental as it forms the basis for the choice of alginate and type of ions to be used. In the present study we indeed show that large variations in Mn^{2+} amount and release are observed for the various alginate gels. In particular, the binding of Mn^{2+} to pure MG sequences is noticeably different from the binding of other alginate samples (Fig. 4 and Table 2). By means of ^{13}C-NMR spectroscopy Emmerichs *et al.* (1) have shown that Mn^{2+} binds to G-blocks in cavities between each pair of G residues in a similar manner to Ca^{2+}, whereas the binding of Mn^{2+} to M-blocks is primarily based on electrostatic attraction without forming stable complexes. Interestingly, in the case of MG-blocks, Mn^{2+} was found to bind specifically and preferentially in a complex owing to the pocket formed by the axial–equatorial link between the two monomers. The macroscopic difference between Mn-gels of polyalternating alginate (rigid and transparent) and alginates containing G-blocks (weak and turbid/white; Fig. 4) demonstrates the distinct binding of Mn^{2+} to MG-blocks. High turbidity and soft texture of gels is a characteristic feature of precipitates as typically seen in Ca-polymannuronate and indicates that the ion binding is not strong enough for the formation of a rigid gel (ordered structure) to be energetically favourable (36). From CD analysis of the three block structures (Fig. 2), there seems to be an interaction of Mn^{2+} with G blocks and, to some extent, with MG blocks, while the CD spectra of polyM are totally unaffected by the additions of the ion, which explains why gels of Mn-polyM alginate could not be formed. However, although the CD spectra point towards

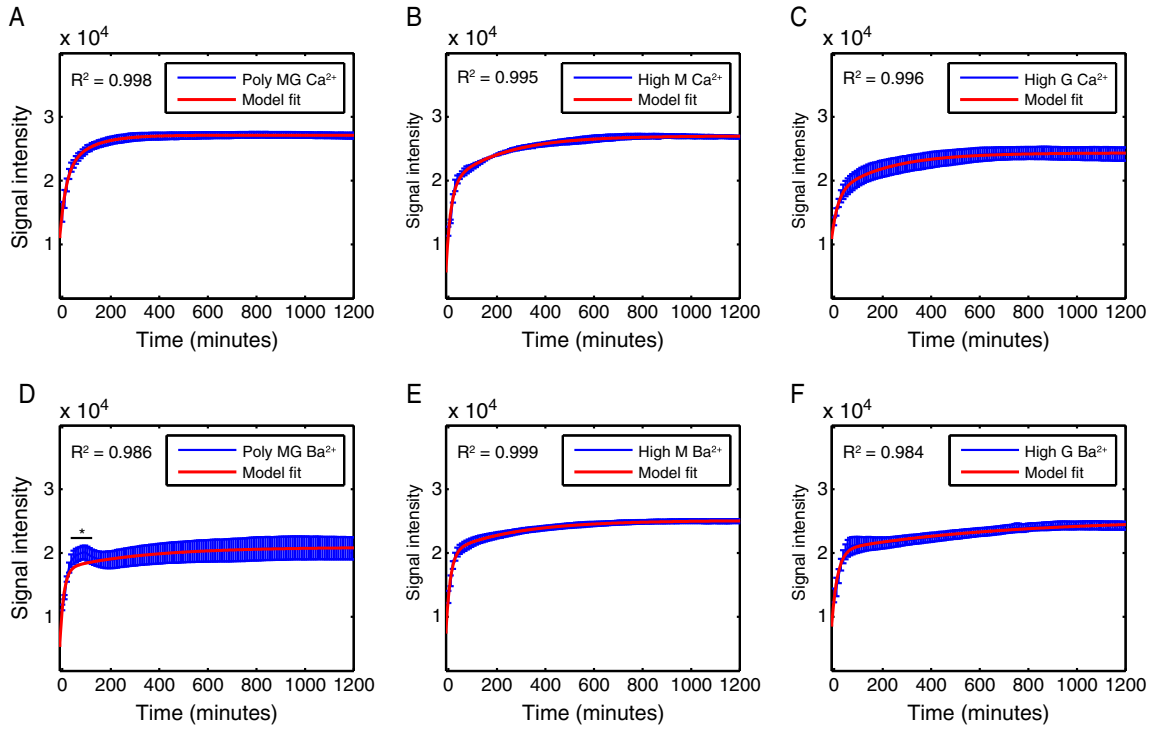

Figure 6. Dynamic MEMRI of (A) PolyMG Mn/Ca-alginate ($n = 6$), (B) high-M Mn/Ca-alginate ($n = 2$), (C) high-G Mn/Ca-alginate ($n = 5$), (D) polyMG Mn/Ba-alginate ($n = 2$), (E) high-M Mn/Ba-alginate ($n = 6$) and (F) high-G Mn/Ba-alginate ($n = 5$). Error bars represent ± SE. The bi-exponential model fitted the data well except for Mn^{2+} release from polyMG Mn/Ba (D) where data points between 47 and 141 min were removed from the fit (*).

Table 3. Time constants (minutes) of Mn^{2+} release from high-G, high-M and polyMG alginate with either Ca^{2+} or Ba^{2+} as stabilizing ions. Values are extracted from bi-exponential fit to dynamic MEMRI (95% confidence intervals in brackets)

		High-G		High-M		PolyMG	
Ca^{2+}	τ_1	219 (209, 229)	$n = 5$	222 (210, 234)	$n = 2$	106 (99, 113)	$n = 6$
	τ_2	25 (22, 28)		19 (17, 21)		24 (22, 26)	
Ba^{2+}	τ_1	677 (555, 799)	$n = 5$	280 (272, 288)	$n = 6$	342 (294, 390)	$n = 2$
	τ_2	23 (21, 25)		18 (17, 19)		16 (14, 18)	

interaction between the ion and the polymer, they do not give information on the nature of the interaction. An additional insight on the overall macromolecular properties of the alginate chain has been attempted by looking at the relative variation of the specific viscosity upon addition of the divalent ions (Fig. 3). The specific viscosity of a polyelectrolyte is strongly affected by the number and distribution of the fixed charges, as well as by their interaction with the mobile counterions. The reduction of the relative specific viscosity upon addition of Mg^{2+} can be interpreted as arising from a combined effect of the dilution of the polymer sample and of the condensation of the divalent cations causing a reduction of the effective charge density and hence a decrease of the polyuronate hydrodynamic volume. Figure 3 shows that the addition of Mn^{2+} ions to the alginate samples analysed leads to a similar trend. Nevertheless, the deviation of relative specific viscosity between Mg^{2+} and Mn^{2+} seems to increase in the order polyM < polyMG < high-G, thus supporting the CD data. However, no alginate sample showed chain-chain association upon addition of Mn^{2+} ions. In fact, when Ca^{2+} ions are added to high-G alginate, a non-monotonic trend of the relative specific viscosity is noticed (Fig. 3C). This has been previously interpreted as an indication of interchain association and network formation (37).

While the findings by Emmerics *et al.* might explain the distinct nature of the Mn-polyMG gel, there is no evidence pointing to Mn^{2+} binding more *strongly* to alternating sequences, as the alginates with high proportions of MG sequences immediately destabilize in saline solution and result in fast release of Mn^{2+}, indicating that Mn^{2+} is quickly exchanged with the non-gelling Na^{+} (Tables 1 and 3 and Fig. 5).

In the present study the highest total amount of divalent ions conserved in the gel after a pre-washing step was, not surprisingly, found in polyG and high-G alginate. These alginates contain long continuous blocks of guluronic acid (G) residues having the highest affinity to divalent ions (38). For the same reason, these alginates are most stable towards swelling and dissolution in saline (Table 1), in particular in combination with Ba^{2+}. Model fitting of the release rate of Mn^{2+} from alginate gels based on MRI scans results in the longest time constants (slowest release) for these gels, confirming our findings on gel stability and divalent ion content studies. However, increasing the G content to almost 90% did not enhance stability further, but

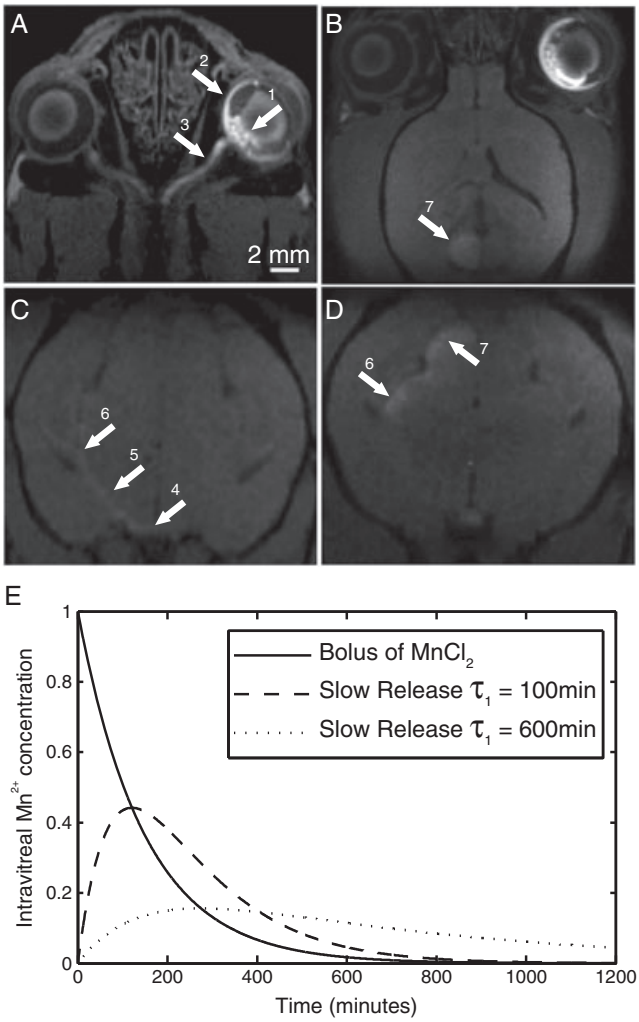

Figure 7. Oblique two-dimensional slices from the three-dimensional MEMRI volume showing the rat retina, optic nerve and contralateral superior colliculus 24 h after *ivit* injection of high-G Ba/Mn alginate beads (1). Mn^{2+} entered the retinal ganglion cells via their Ca^{2+} channels and caused hyperintense signal in the retina (2), optic nerve (3), optic chiasm (4) and further in the contralateral optic tract (5), geniculate nucleus (6) and superior colliculus (7). (E) Simulation of *ivit* Mn^{2+} concentration showed decreased maximum Mn^{2+} concentration as a function of increasing time constant for release. Furthermore, slow release increased the time Mn^{2+} were present in the vitreous body, which increases the time Mn^{2+} are available for retinal ganglion cell uptake *in vivo*.

rather led to the opposite effect, illustrating that a certain proportion of M and MG blocks is required for the formation of stable Mn-alginate hydrogels.

4.2. Effect of secondary stabilizing ions

As Mn^{2+} alone is not sufficient to form a stable alginate hydrogel, secondary divalent ions with higher affinity to alginate must be used. From the present study it is evident that the type of divalent ion chosen for stabilization purposes influences the degree of gel stability to a large extent and can hence be used to manipulate both the amount and release rate of Mn^{2+} from the gel. When a combination of Mn^{2+} and Ca^{2+} is used for gelling a polyalternating alginate, Ca^{2+} will compete with Mn^{2+} because of the rather high specificity of Ca^{2+} to long alternating sequences and formation of MG/MG junctions (2,39). However, as the binding is not strong (40), a large portion of ions (both Mn^{2+} and Ca^{2+}) will be exchanged with Na^{+} during the initial washing procedure of capsules, explaining the low total concentration of ions for this particular gel (Table 2).

The relatively long τ_1 time constant achieved for polyMG alginate with Ba^{2+} deserves comment. As Ba^{2+} is found to bind poorly to polyMG alginate and hence not lead to increased gel stability, a shorter time constant would be expected. However, as our data show (Fig. 6D), Mn^{2+} concentration seems to increase followed by an initial decrease early in the experiment. This could be explained by rapid initial release owing to the very high content of poorly bound Mn^{2+}, which causes local high concentration before Mn^{2+} are distributed in the water volume by diffusion. MR images obtained immediately upon immersion of the alginate beads into NaCl solution corroborate the above observation as they reveal dynamic changes in T_1 consistent with large-scale Mn–Na ion exchange (Fig. 1). In order to describe the slow component of increased Mn^{2+} concentration, data between 47 and 141 min were excluded from the fit and our results may therefore not be representative for Mn^{2+} release from polyMG with Ba^{2+}.

Another interesting observation is the large discrepancy between the Mn^{2+}:Ba^{2+} and Mn^{2+}:Ca^{2+} ratios in the gelling solutions (100:1 and 10:1, respectively) compared with the ratios of ions in the resulting gel beads (Table 2), reflecting the various affinities of ions to alginate. After gelling, the Mn^{2+}:Ca^{2+} ratio was approximately the same for all types of alginates tested, and in all cases Ca^{2+} had accumulated in the gel compared with Mn^{2+}, which was expected given the higher affinity of Ca^{2+} to alginate. In contrast, the Mn^{2+}:Ba^{2+} ratio varied greatly among the alginates studied. The very highest Mn^{2+}:Ba^{2+} ratio was found in the pure polyalternating sample, followed by high-M alginate.

Furthermore, elemental analysis of these gels makes it evident (Table 2) that the amount of bound Ba^{2+} was extremely low compared with alginates with large amounts of G residues. The very low amount of Ba^{2+} bound in gels of polyalternating alginate indicates poor affinity of Ba^{2+} to pure alternating sequences. This explains the limited binding of Ba^{2+} to high-M alginate, also rich in alternating sequences ($F_{GM=MG} = 0.20$). The lack of stability of these alginates in sodium chloride (Table 1) further confirms the above. The findings are consistent with our previous results that indicated poor binding of Ba^{2+} to alternating sequences (6).

4.3. Controlled release of Mn^{2+} for *in vivo* MEMRI

The model fitting showed that Mn^{2+} were released with two different release rates: a fast release rate corresponding to a short time constant and a slow release rate corresponding to a long time constant. The short time constant (τ_2) varied marginally between the different groups of alginate Ba^{2+}/Ca^{2+} combinations and may be attributed to unbound Mn^{2+} precipitated by washing the alginate beads in NaCl prior to MRI data acquisition. Notwithstanding that the initial concentration of Mn^{2+} bound within the gels greatly varies between the different alginates (Table 2), such effects could be reduced by including additional washing steps into our protocol. The substantial longer time constant (τ_1) showed great variation between the groups in the order high-G $\geq$ high-M $>$ polyMG, increasing upon using Ba^{2+} instead of Ca^{2+} as secondary ion. As discussed above, this is consistent with the degree of gel stability of the different types

of alginate and Ba^{2+}/Ca^{2+} combinations. Hence, we interpret τ_1 to be the time constant for release of bound Mn^{2+}.

Ivit injection of Mn-alginate gel beads in rats demonstrates the applicability of alginate gel beads as a slow release system for MEMRI of the CNS. MR image of rat retina, optic nerve and contralateral superior colliculus 24 h post *ivit* injection (Fig. 7A–D) illustrates that Mn^{2+} are indeed released from gel beads in exchange for sodium ions in the vitreous body. The Mn^{2+} are subsequently taken up by retinal ganglion cells (RGC) and transported anterogradely within their axons to the contralateral superior colliculus in the mid brain, similar to what has been demonstrated previously using *ivit* bolus injections of $MnCl_2$ (15,21,22). Simulation of the *ivit* Mn^{2+} concentration after Mn-alginate bead injection (Fig. 7E) shows that a slow release system both reduces the maximum *ivit* Mn^{2+} concentration and increases the time during which Mn^{2+} are available for uptake by RGC. The latter is postulated to increase MR contrast in the Mn^{2+}-enhanced optic nerve (30).

Previously, we have shown that intravitreal bolus injection of 150 nmol $MnCl_2$ yields sufficient contrast at both 2.35 and 7.0 T (21,22). However, longitudinal MEMRI studies that involve repeated intravitreal doses of $MnCl_2$ carry the inherent risk of Mn^{2+}-induced toxicity. Therefore, large reductions in the intravitreal Mn^{2+} can be expected to significantly eliminate potential long-term toxic effects of repeated intravitreal bolus injections of Mn^{2+} on RGC neurons. Based on the findings of our model, we predict that utilization of tailored Mn-alginate beads may achieve reductions of *ivit* Mn^{2+} concentrations of up to ~85%.

Previous work by our group (30) concluded that there is a plateau of maximum Mn^{2+} entry into neurons, suggesting that signal enhancement is contingent on the duration of Mn^{2+} availability rather than on Mn^{2+} dose. Thus, a very important finding in our study is that the slow release mechanism utilizing Mn-alginate beads significantly increases the duration of intravitreal Mn^{2+} availability for uptake by RGC neurons.

The MR T_1 contrast obtained in our study using the Mn-alginate beads was equivalent to the contrast obtained in previous studies using intravitreal bolus injection of $MnCl_2$ (21,22,30,41). However, a thorough investigation and comparison of bolus injections vs Mn-alginate beads in terms of T_1 signal enhancement was beyond the scope of this study, but constitutes one of our future research priorities.

In our model of Mn^{2+} release and subsequent increase of SI in the surrounding water [eqn (6)], we approximated a linear relationship between SI and Mn^{2+} concentration, which is not true for large variations. As Mn^{2+} concentrations gradually increase, the SI tends to underestimate Mn^{2+} concentration and this may have introduced errors in the time constant estimates. However, we believe this to be a systematic error, not interfering with our general conclusions on Mn^{2+} release between the different groups. Future studies should consider time-resolved T_1-mapping for direct measurement of Mn^{2+} concentration.

In both of our compartment models (Fig. 1) we have assumed a concentration-dependent release of Mn^{2+} from the alginate gel beads [eqns (1) and (7)]. In alginate gel, bound Mn^{2+} are released in exchange for Na^+ and are thus dependent on the concentration of the latter. In a closed system, as represented here by an immersed alginate gel in a container, our model seems to be adequate, but in a biological system the supply of Na^+ may be different and our assumption may not be true. However, we believe that our simulation of *ivit* Mn^{2+} concentration clearly demonstrates the potential of reducing Mn^{2+} concentration by use of tailored alginates for slow release of contrast agents.

5. CONCLUSIONS

In the present study we provide proof of concept for Mn-alginate gel beads as potential candidates for slow release of Mn^{2+} in MEMRI applications. Manganese binds to various extents to the different blocks of alginate and the stability of Mn-alginate gels can be further controlled using various secondary ions. Hence, the total amount of manganese in gels as well as the release rate of Mn^{2+} out of gels can be controlled by the choice of alginates and combination of ions. A high-G Mn-alginate stabilized with Ba^{2+} will result in a gel which is stable towards ion exchange and resulting in slow release of manganese, whereas high-M or high-MG alginates will give the opposite. This study can hence form the basis for designing systems for controlled release of Mn^{2+} for MEMRI. Such systems can be tailored to meet specific bioanatomical/biophysical properties of different neuronal populations and experimental models in terms of Mn^{2+} uptake, transport and clearance, while they can be expected to enable significant refinement of the MEMRI technique for safe, non-toxic, serial application in longitudinal studies of CNS damage and repair. Further *in vivo* studies of Mn^{2+} release from alginate capsules constitute a natural progression of our research.

Acknowledgements

The Norwegian Research Council is thanked for funding this work (FUGE MIC Trondheim, Biopolymer Engineering, and a personal grant to Y.A.M.). Y.A.M. further wishes to acknowledge the Chicago Diabetes Project for partly funding the research on ion binding. I.S. wishes to acknowledge funding in support of this work provided by the Medical Imaging Laboratory (MI Lab), Centre for Research-based Innovation, NTNU. The authors are grateful to Dr Berit Strand for fruitful discussions, early planning of experiments and for reading the manuscript. We thank Tina Bugge Pedersen for excellent technical assistance.

REFERENCES

1. Emmerichs N, Wingender J, Flemming HC, Mayer C. Interaction between alginates and manganese cations: identification of preferred cation binding sites. Int J Biol Macromol 2004; 34(1–2): 73–79.
2. Donati I, Holtan S, Mørch YA, Borgogna M, Dentini M, Skjåk-Bræk G. New hypothesis on the role of alternating sequences in calcium-alginate gels. Biomacromolecules 2005; 6(2): 1031–1040.
3. Donati I, Asaro F, Paoletti S. Experimental evidence of counterion affinity in alginates: the case of nongelling ion Mg^{2+}. J Phys Chem B 2009; 113(39): 12877–12886.
4. Haug A, Smidsrød O. Selectivity of some anionic polymers for divalent metal ions. Acta Chem Scand 1970; 24: 843–854.
5. Haug A. The affinity of some divalent metals to different types of alginates. Acta Chem Scand 1961; 15: 1794–1795.
6. Mørch YA, Donati I, Strand BL, Skjåk-Bræk G. Effect of Ca^{2+}, Ba^{2+} and Sr^{2+} on alginate microbeads. Biomacromolecules 2006; 7(5): 1471–1480.
7. Grant GT, Morris ER, Rees DA, Smith PJC, Thom D. Biological interactions between polysaccharides and divalent cations: the egg-box model. FEBS Lett 1973; 32(1): 195–198.
8. Wang ZY, Zhang QZ, Konno M, Saito S. Sol–gel transition of alginate solution by the addition of various divalent-cations – C-13-NMR spectroscopic study. Biopolymers 1993; 33(4): 703–711.

9. Martinsen A, Skjåk-Bræk G, Smidsrød O. Alginate as immobilization material: I. Correlation between chemical and physical properties of alginate gel beads. Biotechnol Bioeng 1989; 33: 79–89.
10. Thu B, Bruheim P, Espevik T, Smidsrød O, Soon-Shiong P, Skjåk-Bræk G. Alginate polycation microcapsules. II. Some functional properties. Biomaterials 1996; 17: 1069–1079.
11. Darrabie MD, Kendall WF, Opara EC. Effect of alginate composition and gelling cation on micro-bead swelling. J Microencapsul 2006; 23(1): 29–37.
12. Zimmermann H, Ehrhart F, Zimmermann D, Muller K, Katsen-Globa A, Behringer M, Feilen PJ, Gessner P, Zimmermann G, Shirley SG, Weber MM, Metze J, Zimmermann U. Hydrogel-based encapsulation of biological, functional tissue: fundamentals, technologies and applications. Appl Phys A Mater Sci Process 2007; 89(4): 909–922.
13. Narita K, Kawasaki F, Kita H. Mn and Mg influxes through Ca channels of motor-nerve terminals are prevented by verapamil in frogs. Brain Res 1990; 510(2): 289–295.
14. Sloot WN, Gramsbergen JBP. Axonal-transport of manganese and its relevance to selective neurotoxicity in the rat basal ganglia. Brain Res 1994; 657(1–2): 124–132.
15. Pautler RG, Silva AC, Koretsky AP. In vivo neuronal tract tracing using manganese-enhanced magnetic resonance imaging. Magn Reson Med 1998; 40(5): 740–748.
16. Watanabe T, Frahm J, Michaelis T. Functional mapping of neural pathways in rodent brain in vivo using manganese-enhanced three-dimensional magnetic resonance imaging. NMR Biomed 2004; 17(8): 554–568.
17. Aoki I, Wu YJL, Silva AC, Lynch RM, Koretsky AP. In vivo detection of neuroarchitecture in the rodent brain using manganese-enhanced MRI. Neuroimage 2004; 22(3): 1046–1059.
18. Aoki I, Tanaka C, Takegami T, Ebisu T, Umeda M, Fukunaga M, Fukuda K, Silva AC, Koretsky AP, Naruse S. Dynamic activity-induced manganese-dependent contrast magnetic resonance imaging (DAIM MRI). Magn Reson Med 2002; 48(6): 927–933.
19. Weng JC, Chen JH, Yang PF, Tseng WYI. Functional mapping of rat barrel activation following whisker stimulation using activity-induced manganese-dependent contrast. Neuroimage 2007; 36(4): 1179–1188.
20. Takeda A, Kodama Y, Ishiwatari S, Okada S. Manganese transport in the neural circuit of rat CNS. Brain Res Bull 1998; 45(2): 149–152.
21. Thuen M, Berry M, Pedersen TB, Goa PE, Summerfield M, Haraldseth O, Sandvig A, Brekken C. Manganese-enhanced MRI of the rat visual pathway: Acute neural toxicity, contrast enhancement, axon resolution, axonal transport, and clearance of Mn^{2+}. J Magn Reson Imag 2008; 28(4): 855–865.
22. Thuen M, Singstad TE, Pedersen TB, Haraldseth O, Berry M, Sandvig A, Brekken C. Manganese-enhanced MRI of the optic visual pathway and optic nerve injury in adult rats. J Magn Reson Imag 2005; 22(4): 492–500.
23. Saleem KS, Pauls JM, Augath M, Trinath T, Prause BA, Hashikawa T, Logothetis NK. Magnetic resonance imaging of neuronal connections in the macaque monkey. Neuron 2002; 34(5): 685–700.
24. Thuen M, Olsen Ø, Berry M, Pedersen TB, Kristoffersen A, Haraldseth O, Sandvig A, Brekken C. Combination of Mn^{2+}-enhanced and diffusion tensor mr imaging gives complementary information about injury and regeneration in the adult rat optic nerve. J Magn Reson Imag 2009; 29(1): 39–51.
25. Olsen Ø, Thuen M, Berry M, Kovalev V, Petrou M, Goa PE, Sandvig A, Haraldseth O, Brekken C. Axon tracing in the adult rat optic nerve and tract after intravitreal injection of MnDPDP using a semiautomatic segmentation technique. J Magn Reson Imag 2008; 27(1): 34–42.
26. Van der Linden A, Van Meir V, Tindemans I, Verhoye M, Balthazar J. Applications of manganese-enhanced magnetic resonance imaging (MEMRI) to image brain plasticity in song birds. NMR Biomed 2004; 17(8): 602–612.
27. van der Zijden JP, Wu O, van der Toorn A, Roeling TP, Bleys R, Dijkhuizen RM. Changes in neuronal connectivity after stroke in rats as studied by serial manganese-enhanced MRI. Neuroimage 2007; 34(4): 1650–1657.
28. Tucciarone J, Chuang KH, Dodd SJ, Silva A, Pelled G, Koretsky AP. Layer specific tracing of corticocortical and thalamocortical connectivity in the rodent using manganese enhanced MRI. Neuroimage 2009; 44(3): 923–931.
29. Brouillet EP, Shinobu L, McGarvey U, Hochberg F, Beal MF. Manganese injection into the rat striatum produces excitotoxic lesions by impairing energy-metabolism. Exp Neurol 1993; 120(1): 89–94.
30. Olsen Ø, Kristoffersen A, Thuen M, Sandvig A, Brekken C, Haraldseth O, Goa PE. Manganese transport in the rat optic nerve evaluated with spatial- and time-resolved magnetic resonance imaging. J Magn Reson Imag 2010; 32: 551–560.
31. Santamaria AB. Manganese exposure, essentiality and toxicity. Indian J Med Res 2008; 128(4): 484–500.
32. Ding DL, Roth J, Salvi R. Manganese is toxic to spiral ganglion neurons and hair cells in vitro. Neurotoxicology 2011; 32(2): 233–241.
33. Gimmestad M, Sletta H, Ertesvåg H, Bakkevig K, Jain S, Suh S, Skjåk-Bræk G, Ellingsen TE, Ohman DE, Valla S. The Pseudomonas fluorescens AlgG protein, but not its mannuronan C-5-epimerase activity, is needed for alginate polymer formation. J Bacteriol 2003; 185(12): 3515–3523.
34. Holtan S, Bruheim P, Skjåk-Bræk G. Mode of action and subsite studies of the guluronan block forming mannuronan C-5 epimerase AlgE1 and AlgE6. Biochem J 2006; 395: 319–329.
35. Haug A, Larsen B, Smidsrød O. Uronic acid sequence in alginate from different sources. Carbohydr Res 1974; 32(2): 217–225.
36. Smidsrød O, Haug A. Properties of poly(1,4-hexuronates) in the gel state. II. Comparison of gels of different chemical composition. Acta Chem Scand 1972; 26: 79–88.
37. Fang YP, Al-Assaf S, Phillips GO, Nishinari K, Funami T, Williams PA, Li LB. Multiple steps and critical behaviors of the binding of calcium to alginate. J Phys Chem B 2007; 111(10): 2456–2462.
38. Smidsrød O. Molecular basis for some physical properties of alginates in the gel state. J Chem Soc Faraday Trans 1974; 57: 263–274.
39. Mørch YA, Donati I, Strand BL, Skjåk-Bræk G. Molecular engineering as an approach to design new functional properties of alginate. Biomacromolecules 2007; 8(9): 2809–2814.
40. Donati I, Mørch YA, Strand BL, Skjåk-Bræk G, Paoletti S. Effect of elongation of alternating sequences on swelling behavior and large deformation properties of natural alginate gels. J Phys Chem B 2009; 113(39): 12916–12922.
41. Sandvig A, Sandvig I, Berry M, Olsen Ø, Pedersen TB, Brekken C, Thuen M. Axonal tracing of the normal and regenerating visual pathway of mouse, rat, frog, and fish using manganese-enhanced magnetic resonance imaging (MEMRI). J Magn Reson Imag 2011; 34(3): 670–675.

